Intelligent Parameter Design-based Impedance Optimization of STATCOM to Mitigate Resonance in Wind Farms

Zhang, Yang; Yang, Y.; Chen, Xin; Gong, Chunying

Published in:
I E E E Journal of Emerging and Selected Topics in Power Electronics

DOI (link to publication from Publisher):
10.1109/JESTPE.2020.3020434

Publication date:
2020

Document Version
Accepted author manuscript, peer reviewed version

Intelligent Parameter Design-based Impedance Optimization of STATCOM to Mitigate Resonance in Wind Farms

Yang Zhang, *Student Member, IEEE*, Yongheng Yang, *Senior Member, IEEE*, Xin Chen, *Member, IEEE*, and Chunying Gong, *Member, IEEE*

***Abstract*—In certain regions and countries, the static synchronous compensator (STATCOM) is required in large-scale wind farms to provide reactive power support. Due to the limitations and complexity in distributed wind power systems, the STATCOM is considered as an effective and cheap alternative for impedance shaping to mitigate resonance. However, there is still a lack of a quantitative stability analysis for practical large-scale wind farms and an optimization approach for the STATCOM impedance to achieve so. Therefore, based on the sequence impedance matrix models of the Type-IV wind turbine generator (WTG) and STATCOM for the network modeling, this paper presents a sequence impedance network-based stability analysis for practical wind farms to accurately reveal the stability of wind farms and quantitatively evaluate the damping provided by the STATCOM. A typical wind farm in Western China is exemplified to demonstrate the proposed stability analysis. Then, an intelligent parameter design-based optimization approach for the STATCOM impedance is proposed, which uses the heuristic intelligence algorithm to solve the STATCOM controller parameters to obtain the optimal stability margin of the wind farm under the constraints of desired performance. Finally, a comparison with the understanding-of-models-based optimization method confirms the efficacy of the proposed impedance optimization approach.**

***Index Terms*— STATCOM, wind farms, impedance modeling, stability analysis, impedance optimization, resonance mitigation.**

I. Introduction

DUE to system operation or regulatory requirements in certain countries and regions, the static synchronous compensator (STATCOM) is practically required in large-scale wind farms for reactive power compensation [1]–[3]. Recently, the STATCOM with additional damping control has been used to suppress the sub-synchronous resonance of wind farms with type-III wind turbine generators (WTGs) [2], [4]. However, like other power electronic devices, the STATCOM may also worsen the stability of the wind farm due to its fast dynamics [5]. Since 2015, sub-synchronous resonances at 20 Hz to 40 Hz and accompanying super-synchronous resonances at 60 Hz to 80 Hz were recorded in Hami, China [6], [7], where Type-IV WTGs and STATCOM are connected to a weak grid. The resonance can trip the system or even damage the WTGs and STATCOM under severe conditions. Eventually, the entire grid stability is challenged.

Resonance is a system problem which depends on both the design of all the converters in wind farms and the impedance of the grid. It can be effectively identified by the impedance-based modeling and analysis [8]–[11], and the resonant issue is usually solved by modifying the control of WTGs to reshape the impedance of the wind farm [12]–[14]. There are, however, situations where it may become ineffective or unfeasible in practice, due to the limitations and complexity caused by the distributed and intermittent nature of renewable (wind) energy [15]. Hence, the STATCOM, which has been directly installed at the point of common coupling (PCC) of wind farms, becomes an effective and cheap alternative for impedance shaping to mitigate resonance. To achieve so, the following should be properly addressed: 1) an impedance-based quantitative stability analysis for practical large-scale wind farms; 2) an optimization approach for the STATCOM impedance.

In the relevant analysis in the literature, the effects of operational conditions, geographical distribution of WTGs, and transmission networks on the stability of wind farms were ignored by simplifying a wind farm into a single converter connected to an infinite grid [8]–[14], [16], [17]. With this, it is difficult to accurately obtain the stability of practical wind farms. Accordingly, a method based on the frequency-domain nodal admittance matrix of multi-machine systems was proposed in [18] and [19]. However, the application of this method is limited to a qualitative analysis of the high-frequency resonance. In [20], all system components of wind farms were represented in the dq-frame impedance models and then lumped based on the network topology, enabling the quantitative stability assessment of both the sub- and super-synchronous frequencies. The impedance model of each component has to be built in (or converted to) a unified

This work was supported in part by the Science and Technology Project of State Grid Corporation of China (SGTYHT/19-JS-215), National Natural Science Foundation of China (51877105), and Jiangsu Postgraduate Research and Practical Innovation Project (KYLX16_0360).

Y. Zhang and X. Chen and C. Gong are with the Jiangsu Key Laboratory of New Energy Generation and Power Conversion, Nanjing University of Aeronautics and Astronautics, Nanjing 210016, China (e-mail: youngzhang@nuaa.edu.cn; chen.xin@nuaa.edu.cn; zjnjgcy@nuaa.edu.cn).

Y. Yang is with the Department of Energy Technology, Aalborg University, Aalborg 9220, Denmark (e-mail: yoy@et.aau.dk).

This article has been accepted for publication in a future issue of this journal, but has not been fully edited. Content may change prior to final publication. Citation information: DOI 10.1109/JESTPE.2020.3020434, IEEE Journal of Emerging and Selected Topics in Power Electronics

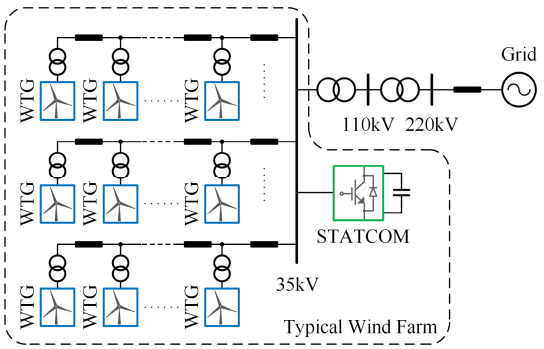

Fig. 1. A typical configuration of a wind farm in Western China.

reference frame before model aggregation, hindering its wide application in scale-up systems. As the sequence impedance is not tied to any local reference frame, the above additional transformation can be avoided using the sequence impedance network modeling presented in [21]. Yet, the assumptions and the complex decoupling between the small signals at perturbation and coupling frequencies [22], [23] make it less applicable. In addition, since the nodal voltages are usually regulated by the STATCOM, the network power flow must be analyzed first, which is not well acknowledged in the above methods.

The STATCOM impedance has been used to provide damping to mitigate resonance, and such damping largely depends on the parameter design [17], [24], [25]. In fact, all STATCOMs have been well-designed to meet the grid connection requirements before installation. However, these designs only focus on the dynamic and steady-state performance of converters without considering the frequency-domain impedance characteristics [26], [27], which may result in a very limited damping effect or even negative damping effect. This can be improved by analyzing the impact of a certain STATCOM control on the system stability and then adding an additional constraint of impedance characteristics corresponding to the STATCOM parameter design [17], [24]. Nevertheless, the effects of these controls on the impedance characteristics, especially at the super- and sub-synchronous frequencies, are coupled with each other [7]. It is thus difficult to shape the STATCOM impedance to generate the optimal damping in wind farms by independently designing its parameters of each control.

With the above concerns, an impedance-based quantitative stability analysis for practical large-scale wind farms, which considers the effects of the steady-state operation trajectory, coupling among WTGs and STATCOM, and network impedances, is presented in this paper to quantitatively evaluate the damping provided by the STATCOM. Then, to achieve resonance mitigation in wind farms, while ensuring the dynamic and steady-state performance of the STATCOM, this paper proposes an optimization approach for the STATCOM impedance. The proposed method adopts the heuristic intelligence algorithms to solve for the STATCOM controller parameters for an optimal stability margin. The rest of the paper is organized as follows. Section II introduces the system configuration. Section III reviews the sequence impedance matrix models of the STATCOM and Type-IV WTG for the network modeling. Section IV presents a quantitative stability analysis for practical wind farms. Section V proposes an optimization approach for the STATCOM impedance to mitigate resonance in wind farms. Finally, Section VI concludes the work.

II. System Configuration

Fig. 1 shows the configuration of the wind farm in Western China, where the WTGs with shunt filter capacitors and 620-V/35-kV step-up transformers are connected in a string. Then, multiple strings are collected at the 35-kV bus to feed power into the transmission network, which is simplified as a transmission cable connected to a voltage source through the 35-kV/110-kV and 110-kV/220-kV transformers. One cascaded H-bridge converter (also called modular multilevel converter in single-star configuration)-based STATCOM is integrated in the wind farm, and it is connected to the 35-kV bus, as presented in Fig. 1.

The circuit and control diagrams of a Type-IV WTG [22] and a STATCOM [28] used in this paper are illustrated in Fig. 2. As shown in Fig. 2(a), since the grid-side converter of the Type-IV WTG is decoupled with its generator-side converter by a dc-link capacitor C_{dc}, the turbine mechanical and generator-side converter can be replaced with a current source, I_{dc}. The control of this WTG includes a dc voltage control, dq-frame phase current control and phase-locked loop (PLL). As shown in Fig. 2(b), since the cell (individual) voltage balancing control does not affect the dynamics of the converter [24], only the average voltage control, phase (clustered) voltage balancing control, dq-frame phase current control, reactive power control and PLL are presented, where v_{ix} (x = a, b, c) indicates the sum of H-bridge module capacitor voltages in each phase.

III. Sequence Impedance Modeling of WTG and STATCOM

To support the impedance-based quantitative stability analysis and the impedance optimization, in this section, the sequence impedance matrix models of the Type-IV WTG and STATCOM developed by the multi-harmonic linearization in [22] and [24], respectively, will be reviewed and the effect of the output terminal dynamics of converters is considered [29].

The sequence impedance modeling can be summarized as follows: first, the steady-state harmonic variables are analyzed by the frequency-domain steady-state model of the converter; then, the small-signal model of the power stage and control of the converter are developed separately; finally, the small-signal model of the control is substituted by the small-signal model of the power stage to obtain the transfer matrix from the vector for the small-signal current response to the vector for the small-signal voltage perturbation, namely, the impedance (admittance) coefficient matrix. Accordingly, the admittance coefficient matrix of the Type-IV WTG in Fig. 2(a) can be expressed as

This article has been accepted for publication in a future issue of this journal, but has not been fully edited. Content may change prior to final publication. Citation information: DOI 10.1109/JESTPE.2020.3020434, IEEE Journal of Emerging and Selected Topics in Power Electronics

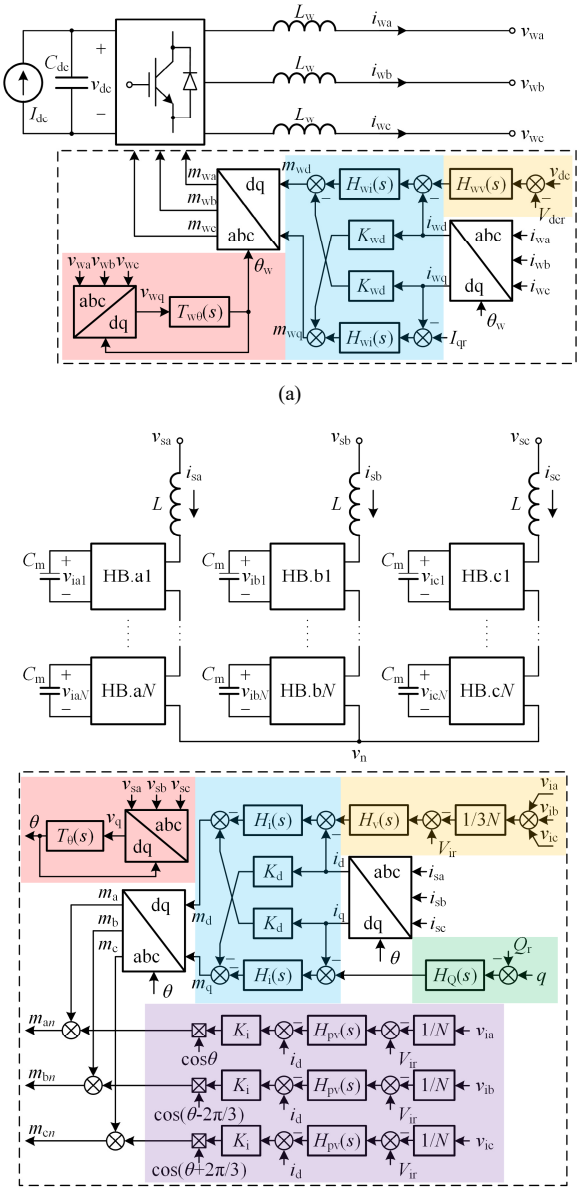

Fig. 2. Circuit and control diagrams of (a) a Type-IV WTG and (b) a cascaded H-bridge STATCOM, where v_{wx} (v_{sx}) represents the output terminal voltages, and i_{wx} (i_{sx}) denotes the phase currents with v_{dc} being the dc-link voltage, L_w being the filter inductor for WTG, and v_{ixn} being the H-bridge module capacitor voltages, L being the arm inductor and C_m being the capacitor in the H-bridge module for STATCOM. (x = a, b, c; n = 1, …, N; HB – H-bridge module).

$$\begin{aligned}\mathbf{Y}_w = &[\mathbf{U}+\frac{1}{2}\mathbf{Y}_{lw}\mathbf{M}_w\mathbf{Z}_{dc}\mathbf{M}_w-\frac{1}{2}\mathbf{Y}_{lw}(\mathbf{V}_{dc}-\mathbf{M}_w\mathbf{Z}_{dc}\mathbf{I}_w)\cdot\\ &(\mathbf{U}+\mathbf{E}_w\mathbf{Z}_{dc}\mathbf{I}_w)^{-1}(\mathbf{Q}_w-\mathbf{E}_w\mathbf{Z}_{dc}\mathbf{M}_w)]^{-1}\mathbf{Y}_{lw}\cdot\\ &[\frac{1}{2}(\mathbf{V}_{dc}-\mathbf{M}_w\mathbf{Z}_{dc}\mathbf{I}_w)(\mathbf{U}+\mathbf{E}_w\mathbf{Z}_{dc}\mathbf{I}_w)^{-1}\mathbf{P}_w-\mathbf{U}]\end{aligned} \quad (1)$$

where $\mathbf{U}$ is the identity matrix, $\mathbf{Y}_{lw}$ is the small-signal admittance of the filter inductor, $\mathbf{Z}_{dc}$ is the small-signal impedance of the dc-link capacitor, and $\mathbf{M}_w$, $\mathbf{I}_w$ and $\mathbf{V}_{dc}$ are the steady-state harmonic matrix for the modulation signal, phase current and dc-link voltage, respectively. Moreover, $\mathbf{E}_w$, $\mathbf{Q}_w$ and $\mathbf{P}_w$ represent the control gain matrix related to the dc-link voltage, phase current and terminal voltage, respectively. Since the negative-sequence admittance coefficient matrix can be obtained by replacing s with $-s$ in the positive-sequence admittance coefficient matrix and then taking the conjugation, only the specific expressions of the above matrices for the positive sequence are presented in Appendix A.

Similarly, the admittance coefficient matrix of the STATCOM presented in Fig. 2(b) is expressed as

$$\begin{aligned}\mathbf{Y}_s = &[(\mathbf{U}+\mathbf{Y}_l\mathbf{M}\mathbf{Z}_c\mathbf{M})+\mathbf{Y}_l(\mathbf{M}\mathbf{Z}_c\mathbf{I}+\mathbf{V}_i)(\mathbf{U}-\mathbf{E}\mathbf{Z}_c\mathbf{I})^{-1}\cdot\\ &(\mathbf{Q}+\mathbf{E}\mathbf{Z}_c\mathbf{M})]^{-1}\mathbf{Y}_l[\mathbf{U}-(\mathbf{M}\mathbf{Z}_c\mathbf{I}+\mathbf{V}_i)(\mathbf{U}-\mathbf{E}\mathbf{Z}_c\mathbf{I})^{-1}\mathbf{P}]\end{aligned} \quad (2)$$

where $\mathbf{Y}_l$ is the small-signal admittance of the arm inductor, $\mathbf{Z}_c$ is the small-signal impedance of the equivalent module capacitor, and $\mathbf{M}$, $\mathbf{I}$ and $\mathbf{V}_i$ are the steady-state harmonic matrix for the insertion index, phase current and the sum of the module capacitor voltages in one phase, respectively. Moreover, $\mathbf{E}$, $\mathbf{Q}$ and $\mathbf{P}$ represent the control gain matrix related to the module capacitor voltage, phase current and terminal voltage, respectively. The specific expressions of the above matrices for the positive sequence can be found in Appendix B.

The elements in the third column of $\mathbf{Y}_w$ or $\mathbf{Y}_s$ indicate that the transfer functions from the voltage perturbation at the angular frequency ω_p to the phase current responses at $\omega_p \pm n\omega_1$ (n = 0, 1, 2; ω_1 is the fundamental angular frequency). Since most of these elements are zero, only the (1, 3)-th (or the (5, 3)-th) and the (3, 3)-th elements are extracted and defined as the transfer function $Y_c(s)$ from the perturbation voltage to the phase current response at the coupling frequency ($\omega_p - 2\omega_1$ for the positive sequence and $\omega_p + 2\omega_1$ for the negative sequence) and the transfer function $Y_p(s)$ from the perturbation voltage to the phase current response at the perturbation frequency ω_p, respectively [10], [22], [30]. Then, according to the relationship between the perturbation voltage and the phase current responses considering the frequency coupling effect [21]–[23] at the output of the converter, the sequence impedance (admittance) matrix model of the Type-IV WTG and STATCOM, can be, respectively, defined as

$$\mathbf{Y}_{WT}(s) = -\begin{bmatrix} Y_{wp}^*(2j\omega_1 - s) & Y_{wc}(s) \\ Y_{wc}^*(2j\omega_1 - s) & Y_{wp}(s) \end{bmatrix} \quad (3)$$

$$\mathbf{Y}_{ST}(s) = \begin{bmatrix} Y_{sp}^*(2j\omega_1 - s) & Y_{sc}(s) \\ Y_{sc}^*(2j\omega_1 - s) & Y_{sp}(s) \end{bmatrix} \quad (4)$$

where the superscript "*" indicates a conjugation.

An example of 4.5-MW WTGs—each WTG is aggregated from three 1.5-MW type-IV WTGs and an example 10-MVA STATCOM are built in MATLAB/Simulink to validate the

This article has been accepted for publication in a future issue of this journal, but has not been fully edited. Content may change prior to final publication. Citation information: DOI 10.1109/JESTPE.2020.3020434, IEEE Journal of Emerging and Selected Topics in Power Electronics

TABLE I
PARAMETERS OF AN EXAMPLE 4.5-MW AGGREGATED WTG

Parameters	Values
Filter Inductance	60 μH
DC-Link Capacitance	90 mF
DC-Link Voltage	1200 V
Grid L-L Voltage (RMS)	620 V @ 50 Hz
Phase Current Controller	$H_{wi}(s) = 7.58\times10^{-5} + 0.163 / s$ $K_{wd} = 3.14\times10^{-5}$
PLL Controller	$H_{w\theta}(s) = 0.18 + 23.11 / s$
DC-Link Voltage Controller	$H_{wv}(s) = 8.573 + 733.02 / s$

TABLE II
PARAMETERS OF AN EXAMPLE 10-MVA STATCOM

Parameters	Values
Number of Modules per Arm	36
Arm Inductance	39 mH
Module Capacitance	1.5 mF
Cell Capacitor Voltage	1000 V
Grid L-L Voltage (RMS)	35 kV @ 50 Hz
Phase Current Controller	$H_i(s) = 6.592\times10^{-4} + 0.415 / s$ $K_d = 3.4\times10^{-4}$
PLL Controller	$H_\theta(s) = 2.95\times10^{-3} + 1.84 / s$
Average Voltage Controller	$H_v(s) = 0.223 + 45.506 / s$
Phase Voltage Balancing Controller	$H_{pv}(s) = 0.0583 + 1.151 / s$ $K_i = 4.538\times10^{-4}$
Reactive Power Controller	$H_Q(s) = 2.375\times10^{-6} + 3.73\times10^{-4} / s$

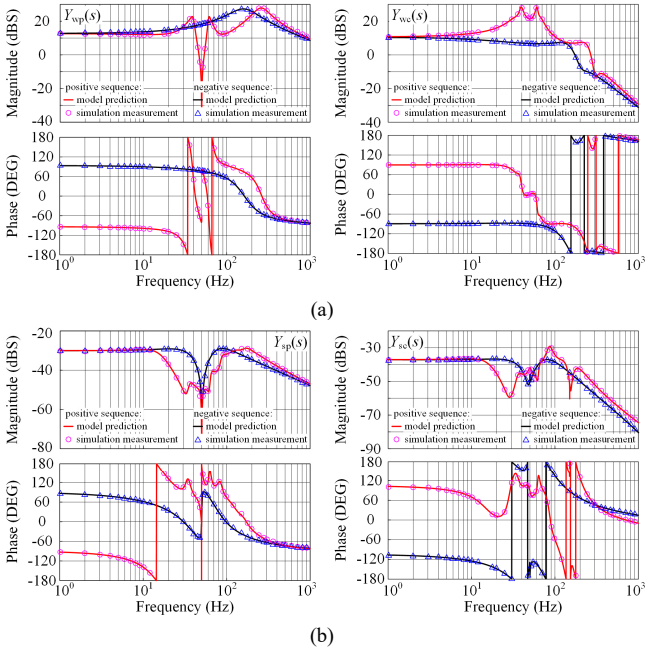

Fig. 3. Frequency responses of the transfer functions for (a) WTG and (b) STATCOM, where the developed models are compared with the time-domain simulation.

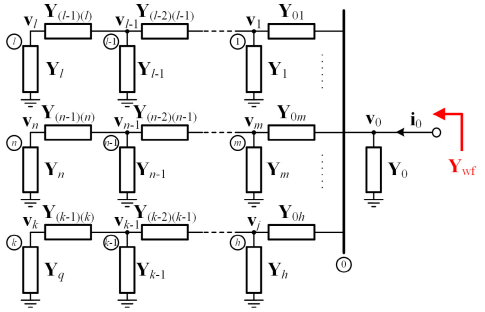

Fig. 4. Impedance (admittance) network of the typical wind farm in Western China.

transfer function $Y_p(s)$ and $Y_c(s)$ in the impedance (admittance) matrix model of (3) and (4), respectively. The parameters of the simulation models are listed in TABLES I and II. A voltage perturbation in either the positive or negative sequence on the output terminal of the converter is injected point by point, and the phase current responses at the corresponding perturbation frequency and coupling frequency is extracted by a Fourier analysis and sequence transformation to calculate the responses of the two transfer functions. Fig. 3 compares the frequency-scanning responses in simulations with the predicted responses based on (3) and (4), respectively. Observations in Fig. 3 indicate that the responses of the developed models and the simulation models are identical over all frequencies.

IV. QUANTITATIVE STABILITY ANALYSIS FOR WIND FARM

To accurately analyze the stability of practical wind farms and quantitatively evaluate the damping provided by the STATCOM impedance, a quantitative stability analysis for the typical wind farm in Western China (see Fig. 1) based on the sequence impedance network, in which the effects of the steady-state operation trajectory, coupling among WTGs and STATCOM, and network impedances are considered comprehensively, is presented in this section.

A. Sequence Impedance Network Modeling

Since the steady-state operating trajectories of an individual converter in practical wind farms are not identical due to many factors, e.g., various wind speeds, impedances of transmission cables and network topologies [15], the power flow calculation should be performed first to obtain the steady-state operating trajectories, including the amplitude and phase of output terminal voltages and the output power as well as the steady-state harmonics of the insertion index, arm current and module capacitor voltage for the MMC [22], [24]. Then, the sequence impedance of each converter in the wind farm can be calculated by substituting their respective steady-state information into the developed small-signal models, and uniformly presented in the matrix form, like (3) and (4). In addition, the impedances of transmission cables and transformers in the wind farm are also required to be represented in a 2×2 matrix, whose first and second diagonal elements corresponding to the small-signal impedance at the coupling frequency and the perturbation frequency. In general, the transformer impedance is developed as its π-type equivalent circuit model, and, the model of transmission cable impedance can be represented, depending on its length, as a series impedance of a π-type equivalent circuit or a standard π-type equivalent circuit or several standard π-type equivalent circuits in series considering the effect of the distributed parameters [31].

This article has been accepted for publication in a future issue of this journal, but has not been fully edited. Content may change prior to final publication. Citation information: DOI 10.1109/JESTPE.2020.3020434, IEEE Journal of Emerging and Selected Topics in Power Electronics

According to the network topology, the impedances of all components of the wind farm including converters, transmission cables and transformers, are connected to develop the impedance model for the entire wind farm, as shown in Fig. 4. The nodes of this impedance network are numbered as 0, 1, …, k–1, k ($1 < l < m < n < h < k$), where the node of the PCC is numbered as 0. Accordingly, the nodal voltage equation of Fig. 4 can be established as

$$\mathbf{Y}_{\mathrm{NW}}(s)\mathbf{v}(s) = \mathbf{y}_0(s)\mathbf{v}_0(s) \tag{5}$$

with $\mathbf{Y}_{\mathrm{NW}}(s)$ being the nodal admittance matrix, whose cells are 2×2 frequency-domain admittance matrices and $\mathbf{v}(s)$ is the nodal voltage matrix, as

$$\mathbf{v}(s) = \left[\mathbf{v}_i(s)\big|_{i=1,2,\cdots,k}\right]^{\mathrm{T}}$$

in which $\mathbf{v}_i(s)$ is the voltage vector of the i-th node. Similarly, $\mathbf{v}_0(s)$ in (5) is the voltage vector of the 0-th node, and $\mathbf{y}_0(s)$ includes admittances between the 0-th node and any other nodes in the network, which is expressed as

$$\mathbf{y}_0(s) = \left[\mathbf{Y}_{0i}(s)\big|_{i=1,2,\cdots,k}\right]^{\mathrm{T}}.$$

Then, based on the Kirchhoff's current law, the current flowing from the 0-th node into the wind farm is obtained as

$$\mathbf{i}_0(s) = [\mathbf{Y}_0(s) + \sum_{i=1}^{k}\mathbf{Y}_{0i}(s)]\mathbf{v}_0(s) - \mathbf{y}_0^{\mathrm{T}}(s)\mathbf{v}(s) \tag{6}$$

Substituting (6) into (5) results in the aggregated admittance of the wind farm that naturally covers the effects of coupling among the converters, line impedances, and network topology:

$$\mathbf{Y}_{\mathrm{wf}}(s) = \mathbf{Y}_0(s) + \sum_{i=1}^{k}\mathbf{Y}_{0i}(s) - \mathbf{y}_0^{\mathrm{T}}(s)\mathbf{Y}_{\mathrm{NW}}^{-1}(s)\mathbf{y}_0(s) \tag{7}$$

B. Quantitative Stability Criteria

Since the sub- and super-synchronous resonances in wind farms are mostly caused by the negative damping effect in the positive-sequence impedance, the following analysis by default considers the positive-sequence case. Based on the definition of the sequence impedance matrix model, the developed admittance for the wind farm $\mathbf{Y}_{\mathrm{wf}}(s)$ and grid-side impedance $\mathbf{Z}_{\mathrm{g}}(s)$ can be defined as

$$\begin{bmatrix} i_1(s) \\ i_2(s) \end{bmatrix} = \begin{bmatrix} Y_{11}(s) & Y_{12}(s) \\ Y_{21}(s) & Y_{22}(s) \end{bmatrix}\begin{bmatrix} v_1(s) \\ v_2(s) \end{bmatrix} = \mathbf{Y}_{\mathrm{wf}}(s)\begin{bmatrix} v_1(s) \\ v_2(s) \end{bmatrix},$$

$$\begin{bmatrix} v_1(s) \\ v_2(s) \end{bmatrix} = -\begin{bmatrix} Z_{11}(s) & Z_{12}(s) \\ Z_{21}(s) & Z_{22}(s) \end{bmatrix}\begin{bmatrix} i_1(s) \\ i_2(s) \end{bmatrix} = -\mathbf{Z}_{\mathrm{g}}(s)\begin{bmatrix} i_1(s) \\ i_2(s) \end{bmatrix}.$$

where $i_1(s) = i_2(s - 2\mathrm{j}\omega_1)$ and $v_1(s) = v_2(s - 2\mathrm{j}\omega_1)$. Then, the stability of such a multi-input-multi-output (MIMO) system can be assessed by applying the generalized Nyquist stability criterion (GNC) to the return-ratio matrix [29]:

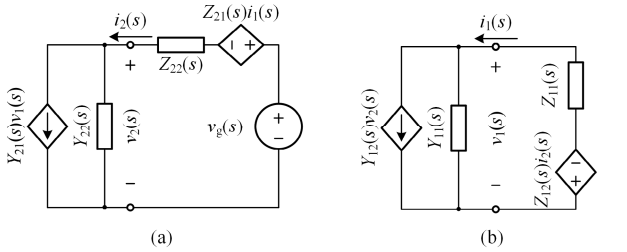

Fig. 5. Equivalent circuit for the responses at the (a) perturbation frequency and (b) coupling frequency.

$$\mathbf{L}(s) = \mathbf{Z}_{\mathrm{g}}(s)\mathbf{Y}_{\mathrm{wf}}(s) \tag{8}$$

However, this criterion can only assess whether the system is stable or not, instead of a quantitative analysis to guide the design for stability.

To overcome this limitation, the MIMO system is disassembled by the frequency of small-signal responses and further illustrated in the two-coupled equivalent circuits for the responses at the perturbation frequency and coupling frequency, respectively, as shown in Fig. 5 [21], [32].

According to Fig. 5, the injected current response at the perturbation frequency can be expressed as

$$i_2(s) = \frac{Y_{\mathrm{ewf}}(s)}{1 + Z_{\mathrm{eg}}(s)Y_{\mathrm{ewf}}(s)}v_{\mathrm{g}}(s) \tag{9}$$

where $Z_{\mathrm{eg}}(s)$ is defined as the equivalent impedance of the grid:

$$Z_{\mathrm{eg}}(s) = Z_{22}(s) - \frac{Z_{12}(s)Z_{21}(s)Y_{11}(s)}{1 + Z_{11}(s)Y_{11}(s)}$$

and $Y_{\mathrm{ewf}}(s)$ is defined as the equivalent admittance of the wind farm:

$$Y_{\mathrm{ewf}}(s) = \frac{Y_{22}(s) - \dfrac{Y_{12}(s)Y_{21}(s)Z_{11}(s)}{1 + Z_{11}(s)Y_{11}(s)}}{[1 + \dfrac{Z_{12}(s)Y_{21}(s)}{1 + Z_{11}(s)Y_{11}(s)}][1 + \dfrac{Z_{21}(s)Y_{12}(s)}{1 + Z_{11}(s)Y_{11}(s)}]}.$$

It is found from (9) that the MIMO system can be equivalent to a decoupled single-input-single-output (SISO) system. Correspondingly, its stability margin can be simply acquired by using the Nyquist criterion (NC) to the equivalent impedance ratio $Z_{\mathrm{eg}}(s)Y_{\mathrm{ewf}}(s)$.

C. Case Study

A wind farm with the configuration referring to Fig. 1 is used to demonstrate the proposed quantitative stability analysis. This wind farm is equipped with one 10-MVA STATCOM and eleven 4.5-MW WTGs. Among these aggregated WTGs, three are connected in the first string, four are connected in the second string, and the rest are connected in the third. The length of power cables used to connect adjacent WTG units in one string and to connect the WTG in

This article has been accepted for publication in a future issue of this journal, but has not been fully edited. Content may change prior to final publication. Citation information: DOI 10.1109/JESTPE.2020.3020434, IEEE Journal of Emerging and Selected Topics in Power Electronics

TABLE III
ELECTRICAL PARAMETERS OF STUDIED WIND FARM SYSTEM

Parameters		Values
620V / 35kV Transformer	Turns Ratio	31/1750
	Short Circuit Impedance	$45.06\times10^{-3}s + 3.54$
35kV / 110kV Transformer	Turns Ratio	7/22
	Short Circuit Impedance	$67.79\times10^{-3}s + 2.66$
110kV / 220kV Transformer	Turns Ratio	1/2
	Short Circuit Impedance	$0.29s + 5.64$
35kV Power Cables	Resistance	0.13 Ω / km
	Inductance	1.27 mH / km
Shunt Filter Capacitance in WTG		1.95 mF

TABLE IV
OPERATION CONDITION OF STUDIED WIND FARM

		Case 1	Case 2	Case 3
Output Power of WTGs in the 1st String / p.u.		0.976	0.976	0.735
Output Power of WTGs in the 2nd String / p.u.		0.922	0.922	0.615
Output Power of WTGs in the 3rd String / p.u.		0.869	0.869	0.495
Output Power of STATCOM / p.u.		0.743	0.829	0.107
220kV Overhead Lines	Equivalent Resistance / Ω	15.08	16.81	15.08
	Equivalent Inductance / H	0.96	1.07	0.96
SCR at the PCC of Wind Farm		2.00	1.87	2.00

the strings to the 35-kV bus is set as 1 km, 5 km, 2 km and 3 km, correspondingly. The parameters of the WTG and STATCOM are shown in TABLES I and II, respectively, and the specifications of other electrical parameters for the wind farm system are listed in TABLE III. Considering the effects of the short circuit ratio (SCR) at the PCC of the wind farm and output power of WTGs on the stability of the wind farm, three cases with different operation conditions of the wind farm are presented in TABLE IV.

Fig. 6 presents the Eigen-loci curve of the return ratio matrix $\mathbf{L}(s)$ for the cases in TABLE IV. In Case 1, there is no right half-plane pole in $\mathbf{L}(s)$ and the trajectory does not enclose the (–1, 0j) point, indicating that the system is stable. In Cases 2 and 3, both trajectories enclose the (–1, 0j) point in a clockwise way, implying instability.

To obtain the quantitative stability margin and more intuitive understanding of the impedance characteristics of the wind farm, the MIMO system is further transferred to the SISO system based on Fig. 5, and the equivalent impedance ratio $Z_{eg}(s)Y_{ewf}(s)$ is presented in the Bode diagram, as shown in Fig. 7, where $Z_{ewf}(s) = Y_{ewf}(s)^{-1}$. In Case 1, the phase margin at the intersection frequency (94.7 Hz) of $Z_{ewf}(s)$ and $Z_{eg}(s)$ is 2.55°, which means that the system is stable but has less damping. In Case 2, the SCR at the PCC of the wind farm decreases while the output power of WTGs remains unchanged and the STATCOM generates more reactive power to maintain the PCC voltage, which affects the low-frequency impedance characteristics of $Z_{ewf}(s)$ below 20 Hz. Accordingly, the intersection frequency of $Z_{ewf}(s)$ and $Z_{eg}(s)$ shifts to 91.4 Hz with –1.72°-phase margin caused by the negative resistance characteristics in $Z_{ewf}(s)$. This indicates

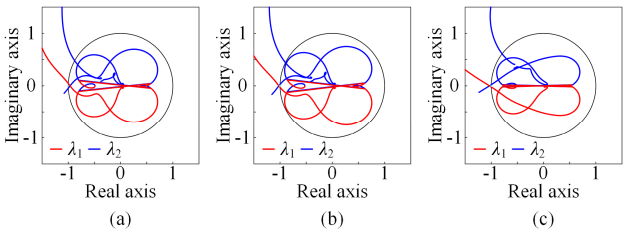

Fig. 6. Eigen-loci curve of the return ratio matrix **L** for (a) Case 1, (b) Case 2, and (c) Case 3.

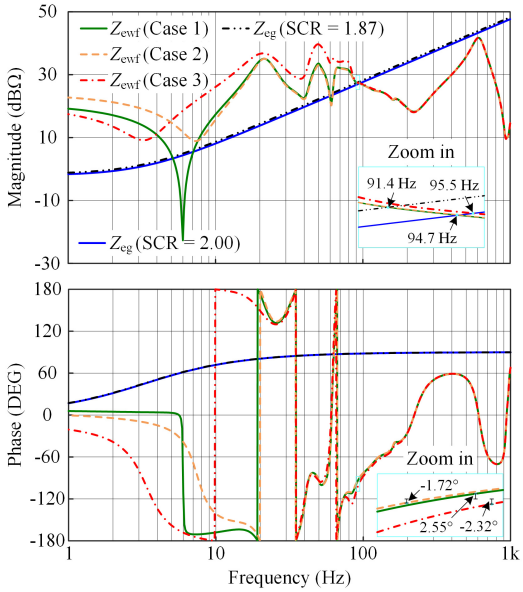

Fig. 7. Sequence impedance responses of Z_{ewf} and Z_{eg} for studied cases.

that the system is unstable. In Case 3, the SCR is the same as in Case 1, but the output power of WTGs and STATCOM is reduced. The amplitude responses of $Z_{ewf}(s)$ around the fundamental frequency increase significantly, but its corresponding phase decreases slightly, which leads to an intersection at 95.5 Hz between $Z_{ewf}(s)$ and $Z_{eg}(s)$ with –2.32°-phase margin. Obviously, such a system is also unstable.

Fig. 8 shows the simulation results for the PCC voltages, injected currents, and output power of the wind farm. As observed in Fig. 8(a) for Case 1, there are no significant harmonics in the PCC voltages and injected currents and no oscillations on the active power and reactive power either, which are consistent with the fast Fourier transformation (FFT) results of the injected currents in Fig. 9. For Cases 2 and 3, resonances occur and gradually diverge in the PCC voltages, injected currents, and output power of the wind farm, as shown in Figs. 8 (b) and (c). The FFT results for the injected currents presented in Fig. 9 identify the dominant resonance frequencies are 92 Hz and 96 Hz, and their magnitudes are up to 6.37% and 8.91% of the fundamental, respectively. These time-domain simulation results all agree with the analysis in Figs. 6 and 7, which confirms the effectiveness of the proposed quantitative stability analysis for practical large-scale wind farms.

This article has been accepted for publication in a future issue of this journal, but has not been fully edited. Content may change prior to final publication. Citation information: DOI 10.1109/JESTPE.2020.3020434, IEEE Journal of Emerging and Selected Topics in Power Electronics

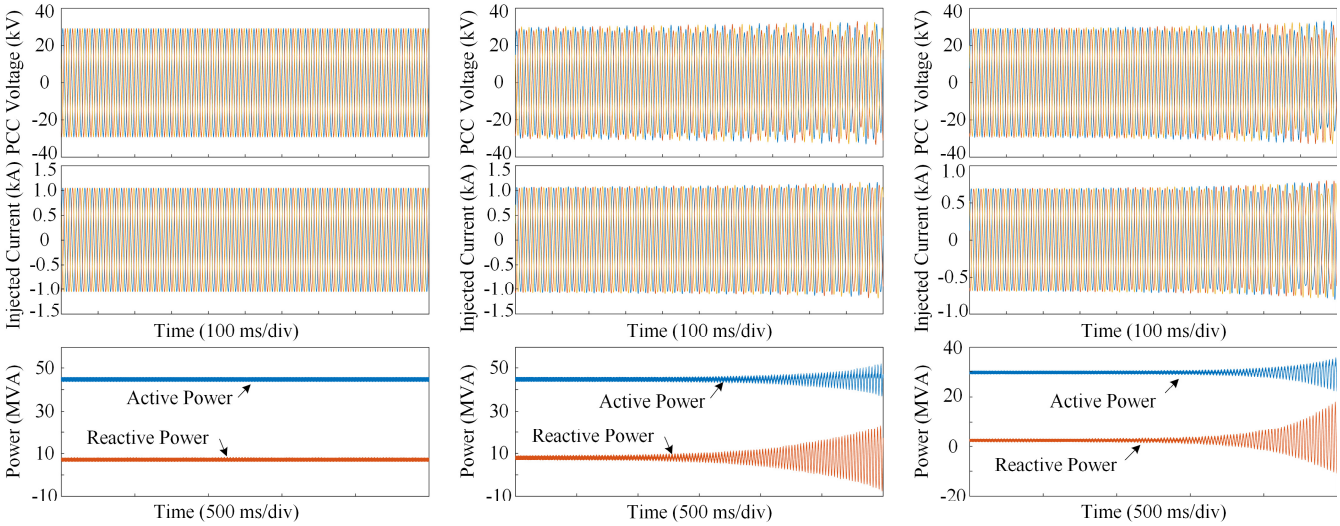

Fig. 8. Simulation results of the PCC voltages, injected currents, and output powers of the studied wind farm for (a) Case 1, (b) Case 2, and (c) Case 3.

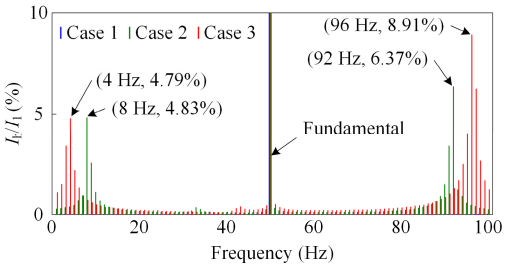

Fig. 9. FFT results of the injected currents of the wind farm for studied cases (Fig. 8).

V. STATCOM Impedance Optimization

A. Effect of Controls on STATCOM Impedance

Since the effect of STATCOM impedance on the system stability depends on its parameters [17], [24], a brief review for the parameter design of the dq-frame phase current control, PLL, average voltage control and reactive power control in the STATCOM is presented first to understand the relationship between the performance indices of each control loop in the parameter design and the STATCOM impedance characteristics. The transfer function diagrams of these control loops are illustrated in Fig. 10, where V_{i0} is the dc component of the sum of the module capacitor voltages in one phase and $G_{icl}(s)$ is the closed-loop transfer function of the dq-frame phase current control loop. The closed-loop transfer function can be simplified as $G_{icl}(s) \approx 1$, as the outer loop (i.e., the average voltage control and the reactive power control) is much slower than the inner loop (i.e., the dq-frame phase current control).

Based on Fig. 10, the open-loop gain of the dq-frame phase current control, PLL and average voltage control is given as

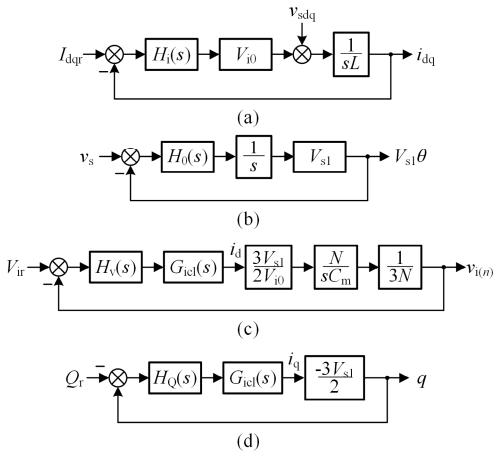

Fig. 10. Transfer function diagrams of the (a) dq-frame phase current control loop; (b) PLL; (c) average voltage control loop; and (d) reactive power control loop.

$$G_{ol}(s) = GH_1(s)/s \tag{10}$$

where $H_1(s) = K_{p1} + K_{i1}/s$ is a proportional-integral (PI) regulator and $G = V_{i0}/L$ is a proportional gain for the dq-frame phase current control. More specifically, $G = V_{s1}$ for the PLL and $G = V_{s1}/(2V_{i0}C_m)$ for the average voltage control (V_{s1} is the amplitude of the fundamental output voltage).

According to (10), the closed-loop of these three controls is a second-order system, and then, the system can be designed by its bandwidth ω_b and the phase margin γ ($\gamma > 0$) at the gain crossover frequency ω_x of (10) to meet the requirements of the dynamic and steady-state performance. Then, there is

$$\begin{cases} \left| G_{ol}(j\omega_b)/(1+G_{ol}(j\omega_b)) \right| = 1/\sqrt{2} \\ \arg(G_{ol}(j\omega_x)) + \pi = \gamma \end{cases} \tag{11}$$

This article has been accepted for publication in a future issue of this journal, but has not been fully edited. Content may change prior to final publication. Citation information: DOI 10.1109/JESTPE.2020.3020434, IEEE Journal of Emerging and Selected Topics in Power Electronics

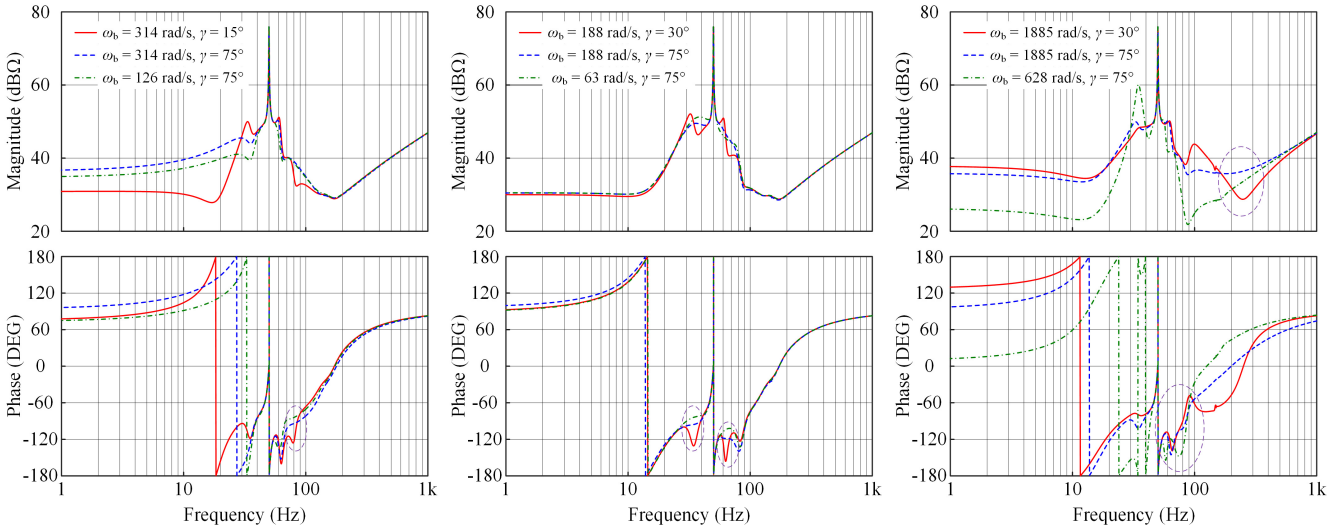

Fig. 11. Comparison of the STATCOM impedance responses ($Y_{sp}(s)^{-1}$) for the (a) PLL, (b) average voltage control, and (c) dq-frame phase current control in different parameter designs, respectively.

where ω_x can be obtained by solving $|G_{ol}(j\omega_x)| = 1$. Solving (11) gives

$$\omega_b = \frac{\sqrt{2}GK_{p1}}{\Phi(\gamma)} \tag{12.1}$$

$$\varphi(\gamma) = \frac{GK_{p1}^2}{K_{i1}} \tag{12.2}$$

with $\Phi(\gamma) = \sqrt{\varphi(\gamma)(-\varphi(\gamma) - 2 + \sqrt{(\varphi(\gamma)+2)^2 + 4})}$ and $\varphi(\gamma) = \tan(\gamma)\sin(\gamma)$.

Furthermore, the open-loop gain of the reactive power control can be written as

$$G_{ol}(s) = GH_2(s) \tag{13}$$

in which $H_2(s) = K_{p2} + K_{i2}/s$ is a PI regulator and $G = 1.5V_{s1}$.

With the closed-loop system in (11), it can be obtained as

$$\omega_b = \frac{GK_{p2}}{T_i\sqrt{2-(GK_{p2}-1)^2}} \tag{14.1}$$

$$T_i = \frac{K_{p2}}{K_{i2}} \tag{14.2}$$

where T_i is the integral time constant.

Based on this design principle, the parameters of the PI regulator in the dq-frame phase current control, PLL, average voltage control and reactive power control can be determined by substituting the desired performance indices (the bandwidth ω_b and the phase margin γ or integral time constant T_i) into (12) or (14). Fig. 11 compares the sequence impedance response ($Y_{sp}(s)^{-1}$) of the STATCOM presented in Section III by respectively regulating the parameters of the PLL, average voltage control and dq-frame phase current control.

As shown in Fig. 11(a), the fast PLL introduces a significant negative damping effect on the impedance responses, which sharply decreases the phase and then challenges the stability of the entire wind farm. Moreover, in the situation that the bandwidth of the PLL is identical, the impedance characteristics will vary with the different phase margins. Specifically, the PLL with a low phase margin will limit the negative damping effect to a relatively small frequency range that is usually below its bandwidth frequency but lead to more dipping on both the magnitude and phase responses at these frequencies. On the contrary, the PLL with a high phase margin will slightly decrease the phase responses in a wider frequency range. In fact, it is difficult to conclude arbitrarily whether the PLL with a low or high phase margin is desired for the system stability, since the STATCOM with a low-phase-margin PLL can provide more damping at the potential resonance frequency than it with a high-phase-margin PLL, as long as the frequency of the "dip" on the phase responses is less than that potential resonance frequency.

The effect of the average voltage control loop with different parameter designs on the phase response of the STATCOM impedance is similar to that of the PLL, except that its effect on the magnitude responses is much weaker, as observed in Fig. 11(b).

The magnitude responses of the STATCOM impedance are mainly affected by the bandwidth of the dq-frame phase current control loop, and in general, the wider the bandwidth is, the greater the magnitude responses will be, as shown in Fig. 11(c). Additionally, when the current control loop is too slow and the PLL and average voltage control loop is too fast,

This article has been accepted for publication in a future issue of this journal, but has not been fully edited. Content may change prior to final publication. Citation information: DOI 10.1109/JESTPE.2020.3020434, IEEE Journal of Emerging and Selected Topics in Power Electronics

the impedance characteristics below 100 Hz will be dominated by the latter two, showing a negative damping effect. The effect of the phase margin in the dq-frame phase current control loop on the impedance responses is also presented in Fig. 11(c). The current control loop with a higher phase margin provides more damping to the STATCOM impedance near the bandwidth frequency, which may enhance the system stability in the case that the bandwidth frequency of the current control loop is close to the potential resonance frequency.

Based on the above analysis and Fig. 11, it can be found that the STATCOM impedance characteristics in certain frequency ranges, especially at the sub- and super-synchronous frequencies, may be affected by more than one control loops. Furthermore, these effects on the impedance responses caused by each control loop are not linearly superimposed, but coupled with each other. This makes it difficult to obtain the optimal STATCOM impedance responses for the system stability improvement by tuning the parameters either in only one of the control loops or in several control loops.

On the other hand, the optimization of the STATCOM impedance to mitigate resonance in wind farms is just an additional function for the STATCOM. Focusing only on the effect of each STATCOM control loop on the impedance responses, regardless of the rationality of its parameter design, may compromise the dynamic and steady-state performance of the STATCOM, or even fail to perform its basic function, which should be avoided.

B. Intelligent Parameter Design-Based Impedance Optimization

With the above considerations, an intelligent parameter design-based optimization approach for the STATCOM impedance is proposed. In this approach, the parameter co-design for multiple STATCOM control loops is formulated as a combinatorial optimization problem, where the objective is to find the maximum stability margin of the equivalent impedance ratio of the wind farm system and it is restricted by the dynamic and steady-state performance of the STATCOM.

(1) *Objective Function*

Based on the quantitative stability analysis in Section IV, the phase margin of the equivalent impedance ratio $Z_{eg}(s)Y_{ewf}(s)$ at the angular frequency ω_{co} that the Nyquist curve intersects with the unit circle, namely, the system stability margin (Phase Margin - PM), is introduced as the objective function, which is

$$\mathrm{PM} = \pi - \arg(Z_{eg}(\mathrm{j}\omega_{co})Y_{ewf}(\mathrm{j}\omega_{co})) \tag{15}$$

in which the intersection frequency ω_{co} can be obtained by solving $|Z_{eg}(\mathrm{j}\omega_{co})Y_{ewf}(\mathrm{j}\omega_{co})| = 1$.

(2) *Constraints*

In this optimization approach, the constraints are associated with the performance indices (the bandwidth and the phase margin or integral time constant) to ensure the STATCOM with the controller parameters obtained by the optimal design to meet a basic requirement of the dynamic and steady-state performance. It is assumed that the desired performance indices for the control loops are defined as

$$\omega_b \in [\omega_{bmin}, \omega_{bmax}],\ \gamma \in [\gamma_{min}, \gamma_{max}],\ T_i \in [T_{imin}, T_{imax}].$$

Based on (12.1) and (14.1), the function for the proportional coefficient can be defined respectively as

$$f_{Kp1}(\omega_b, \gamma) = \frac{\omega_b \Phi(\gamma)}{\sqrt{2}G} \tag{16}$$

$$f_{Kp2}(\omega_b, T_i) = \frac{1}{G(\sqrt{2 + 1/(T_i\omega_b)^2} - 1)} \tag{17}$$

Since $\Phi(\gamma)$ in (16) is a monotonically increasing function for $\gamma \in (0, \pi/2)$, the constraints of the proportional coefficient K_{p1} in the PI regulator of the dq-frame phase current control, PLL and average voltage control is expressed as

$$K_{p1} \in \left[f_{Kp1}(\omega_{bmin}, \gamma_{min}), f_{Kp1}(\omega_{bmax}, \gamma_{max}) \right] \tag{18}$$

Based on (17), the constraints of the proportional coefficient K_{p2} in the PI regulator of the reactive power control becomes

$$K_{p2} \in \left[f_{Kp2}(\omega_{bmin}, T_{imin}), f_{Kp2}(\omega_{bmax}, T_{imax}) \right] \tag{19}$$

The upper and lower bounds of the integral coefficient can also be obtained based on a similar analysis. However, they cannot serve as constraints of the integral coefficient. In fact, when one of the coefficients in the PI regulator is determined, the range of the performance indices available for designing another coefficient will be limited to meet both requirements of the bandwidth and the phase margin or integral time constant. Therefore, based on (12.2) and (14.2), the constraints of the integral coefficient are designed as a function related to the proportional coefficient.

Specifically, for a given proportional coefficient, there is a minimum available bandwidth, denoted as ω_{cbmin}, by substituting $\varphi(\gamma_{max})$ and T_{imax} into (12.1) and (14.1). By comparing the minimum available bandwidth ω_{cbmin} with the minimum desired bandwidth ω_{bmin}, the available maximums of $\varphi(\gamma)$ and T_i that satisfy the requirement of the bandwidth can be, respectively, expressed as

$$\varphi(\gamma_{cmax}) = \begin{cases} \dfrac{2A_1 + A_1\sqrt{8 - 2A_1}}{4 - 2A_1}, & \omega_{cbmin} < \omega_{bmin} \\ \varphi(\gamma_{max}), & \omega_{cbmin} \geq \omega_{bmin} \end{cases} \tag{20}$$

$$T_{cimax} = \begin{cases} \dfrac{GK_{p2}}{\omega_{bmin}\sqrt{2 - (GK_{p2} - 1)^2}}, & \omega_{cbmin} < \omega_{bmin} \\ T_{imax}, & \omega_{cbmin} \geq \omega_{bmin} \end{cases} \tag{21}$$

This article has been accepted for publication in a future issue of this journal, but has not been fully edited. Content may change prior to final publication. Citation information: DOI 10.1109/JESTPE.2020.3020434, IEEE Journal of Emerging and Selected Topics in Power Electronics

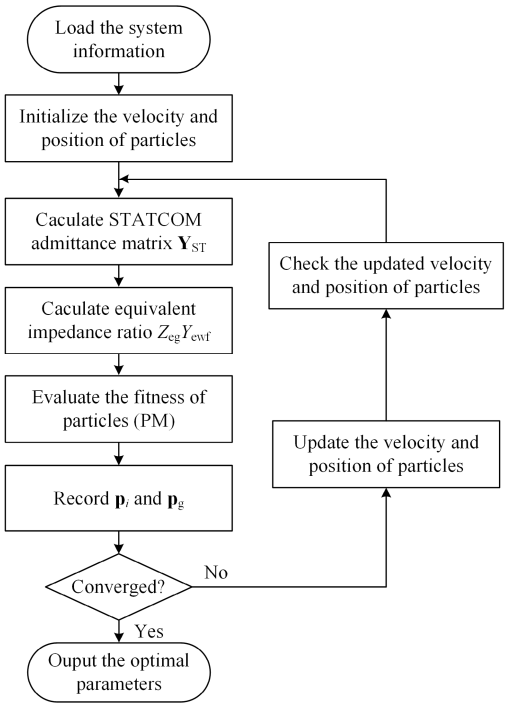

Fig. 12. Flowchart of the implementation of the proposed intelligent parameter design-based optimization approach.

in which $A_1 = 2G^2K_{p1}^2/\omega_{bmin}^2$. Similarly, there will be a maximum available bandwidth, denoted as ω_{cbmax}, by taking $\varphi(\gamma_{min})$ and T_{imin} into (12.1) and (14.1). The available minimums of $\varphi(\gamma)$ and T_i that satisfy the requirement of the bandwidth can be obtained as

$$\varphi(\gamma_{cmin}) = \begin{cases} \dfrac{2A_2 + A_2\sqrt{8-2A_2}}{4-2A_2}, & \omega_{cbmax} > \omega_{bmax} \\ \varphi(\gamma_{min}), & \omega_{cbmax} \le \omega_{bmax} \end{cases} \quad (22)$$

$$T_{cimin} = \begin{cases} \dfrac{GK_{p2}}{\omega_{bmax}\sqrt{2-(GK_{p2}-1)^2}}, & \omega_{cbmax} > \omega_{bmax} \\ T_{imin}, & \omega_{cbmax} \le \omega_{bmax} \end{cases} \quad (23)$$

in which $A_2 = 2G^2K_{p1}^2/\omega_{bmax}^2$.

Based on the above, the constraints of the integral coefficient K_{i1} in the PI regulator of the dq-frame phase current control, PLL and average voltage control is expressed as

$$K_{i1} \in \left[GK_{p1}^2 / \varphi(\gamma_{cmax}), GK_{p1}^2 / \varphi(\gamma_{cmin}) \right] \quad (24)$$

The constraints of the integral coefficient K_{i2} in the PI regulator of the reactive power control is

$$K_{i2} \in \left[K_{p2} / T_{cimax}, K_{p2} / T_{cimin} \right] \quad (25)$$

(3) *Implementation by PSO Algorithm*

TABLE V
PERFORMANCE REQUIREMENTS AND RELATED PARAMETERS USED IN PSO

Parameters		Values
dq-frame Current Control	Control Bandwidth ω_b	$[2\omega_1, 6\omega_1]$
	Phase Margin γ	$[\pi/6, \pi/3]$
Phase-Locked Loop	Control Bandwidth ω_b	$[\omega_1/5, \omega_1]$
	Phase Margin γ	$[\pi/6, \pi/3]$
Average Voltage Control	Control Bandwidth ω_b	$[\omega_1/5, 3\omega_1/5]$
	Phase Margin γ	$[\pi/6, \pi/3]$
Reactive Power Control	Control Bandwidth ω_b	$[2\omega_1/5, 4\omega_1/5]$
	Time Constant T_i	[1/200, 1/100]
Swarm Size m		100
Inertia Weight ω		0.8
Particle Cognitive Learning Factor c_1		2
Swarm Social Learning Factor c_2		2
Number of Iterations		100

TABLE VI
IMPROVED AND OPTIMAL STATCOM CONTROLLER PARAMETERS

Parameters	Values	
	Conventional Optimization	Proposed Optimization
$H_i(s)$	$1.737\times10^{-3} + 0.499/s$	$4.298\times10^{-4} + 0.114/s$
$H_\theta(s)$	$8.683\times10^{-4} + 5.98\times10^{-3}/s$	$7.238\times10^{-4} + 0.0519/s$
$H_v(s)$	$0.0936 + 0.643/s$	$0.0782 + 5.60/s$
$H_Q(s)$	$2.04\times10^{-5} + 2.04\times10^{-3}/s$	$4.97\times10^{-5} + 4.97\times10^{-3}/s$

This optimization problem can be easily solved by heuristic intelligence algorithms, such as the genetic algorithm, simulated annealing algorithm, and particle swarm optimization (PSO) algorithm [33]. In this paper, the PSO algorithm that has been used in the parameter optimization for WTGs [34], [35] and HVDC converters [36], [37] is exemplified to illustrate the proposed intelligence parameter design approach, as shown in Fig. 12. Notably, others can also be used. The first step is to load the system information, including the configuration, electrical parameters, and steady-state operating trajectories of the wind farm. Then, a swarm of m particles are generated randomly in the feasible region of the solution space defined by (18) or (19) and (24) or (25), in which the position of the particle $\mathbf{x}_i$ (i = 1, 2, …, m) represents four pairs of parameters in the PI regulator of the dq-frame phase current control, PLL, average voltage control, and reactive power control, respectively, and the velocity of the particle $\mathbf{v}_i$ represents the change step of these parameters. These controller parameters combined with the obtained system information are used to calculate the STATCOM admittance coefficient matrix $\mathbf{Y}_{ST}$ and the equivalent impedance ratio $Z_{cg}Y_{ewf}$ of the wind farm, which in turn evaluates the fitness of particles, that is, the system stability margin PM in (15). Each particle records the best position (namely, the set of controller parameters that maximizes the PM) achieved by itself $\mathbf{p}_i$ and the entire swarm $\mathbf{p}_g$. The particles are updated based on the evolution equations of the PSO algorithm, expressed as

$$\mathbf{v}_i(t+1) = \omega\mathbf{v}_i(t) + c_1r_1(\mathbf{p}_i - \mathbf{x}_i(t)) + c_2r_2(\mathbf{p}_g - \mathbf{x}_i(t)) \quad (26)$$

$$\mathbf{x}_i(t+1) = \mathbf{x}_i(t) + \mathbf{v}_i(t+1) \quad (27)$$

This article has been accepted for publication in a future issue of this journal, but has not been fully edited. Content may change prior to final publication. Citation information: DOI 10.1109/JESTPE.2020.3020434, IEEE Journal of Emerging and Selected Topics in Power Electronics

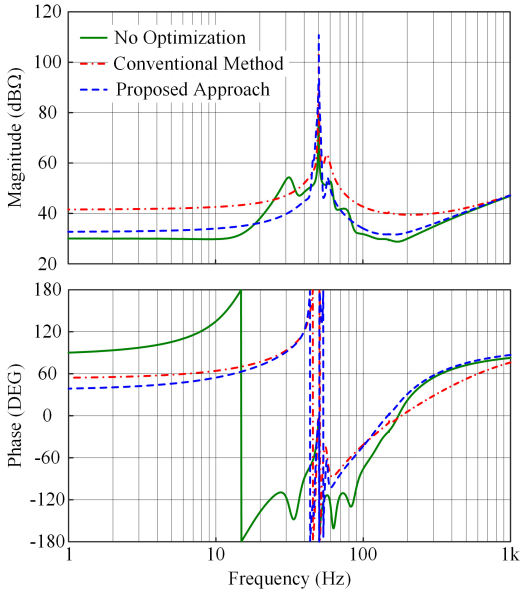

Fig. 13. STATCOM impedance responses ($Y_{sp}(s)^{-1}$) with different sets of controller parameters.

where t denotes the number of iterations, ω represents the inertia weight, two positive constants c_1 and c_2 represent the particle cognitive learning factor and the swarm social learning factor, and r_1 and r_2 are random parameters within [0, 1]. Once updated, the particles go through the feasibility check to ensure that no particle flies outside the feasible region. The above steps will be repeated until the preset number of iterations is reached, and the set of optimal controller parameters is generated for the STATCOM impedance shaping.

C. Comparison and Discussion

In this section, the optimization of the STATCOM impedance in the studied wind farm with the operation condition in Case 2 (see Section IV.D) is used to demonstrate the proposed intelligent parameter design approach, where the performance requirements for each STATCOM control and the related parameters used in the PSO algorithm are listed in TABLE V. After reaching the preset number of iterations, the best fitness (PM) converges to 25.21°, and the corresponding STATCOM controller parameters to achieve this optimal stability margin under these performance requirements are presented in TABLE VI. On the other hand, to compare with the proposed approach, the STATCOM impedance is also optimized by understanding the effects of the performance indices of each control loop on the impedance characteristics. A large phase margin or a slow integral time constant while minimizing the bandwidth of the PLL, average voltage control loop, and reactive power control loop and increasing the bandwidth of the dq-frame phase current loop is used in this optimal design to reduce the negative damping effect on the STATCOM impedance responses at the sub- and super-synchronous frequencies. The corresponding STATCOM controller parameters are also presented in TABLE VI, denoted as "Conventional Optimization".

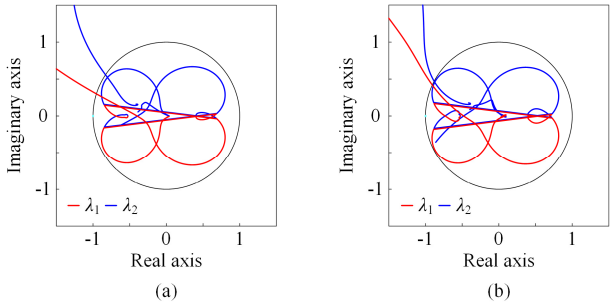

Fig. 14. Eigen-loci curve of the return ratio matrix **L** for the STATCOM optimized by the (a) conventional method and (b) proposed approach.

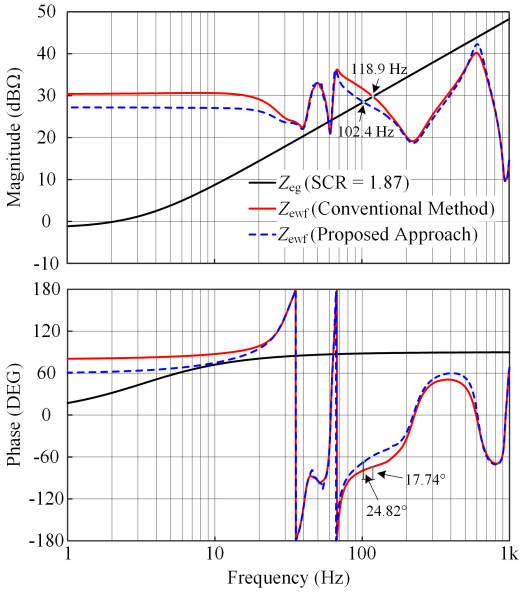

Fig. 15. Sequence impedance responses of Z_{ewf} and Z_{eg} for the STATCOM optimized by the conventional method and proposed approach.

Fig. 13 presents the sequence impedance responses ($Y_{sp}(s)^{-1}$) of the STATCOM with the controller parameters listed in TABLE II (denoted as "No Optimization") and TABLE VI, respectively. Compared to the STATCOM impedance responses without optimization, the phase responses of the STATCOM with other two sets of controller parameters below 200 Hz are increased significantly. Specifically, there are no negative damping effects on the impedance responses of the STATCOM optimized by the conventional method at the low frequencies except for those close to the fundamental frequency, but the phase of the impedance response of the STATCOM optimized by the proposed approach is still below –90° at about 60 Hz, showing the negative damping effect. Additionally, the magnitude of the former impedance responses is much larger than the latter, which implies that the STATCOM optimized by the conventional method has lower harmonics in the output phase currents.

Based on the quantitative stability analysis for the wind farm presented in Section IV, the stability of the wind farm for the STATCOM optimized by the conventional method and proposed approach is assessed by the Eigen-loci curve of the return ratio matrix **L**(s), as presented in Fig. 14. It can be seen

This article has been accepted for publication in a future issue of this journal, but has not been fully edited. Content may change prior to final publication. Citation information: DOI 10.1109/JESTPE.2020.3020434, IEEE Journal of Emerging and Selected Topics in Power Electronics

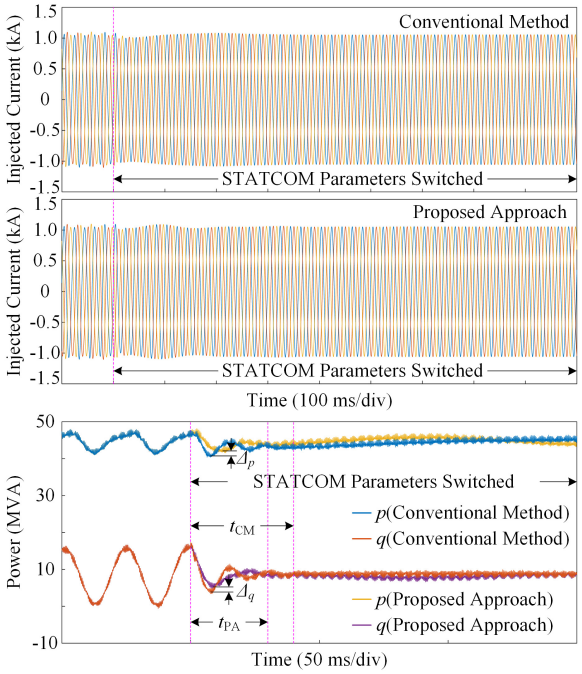

Fig. 16. Simulation results of the injected currents and output powers of the studied wind farm for the STATCOM optimized by the conventional method and proposed approach.

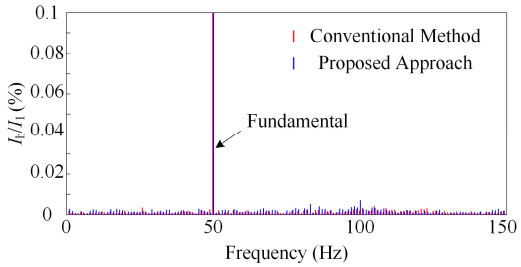

Fig. 17. FFT results of the injected currents of the wind farm for the STATCOM optimized by the conventional method and proposed approach.

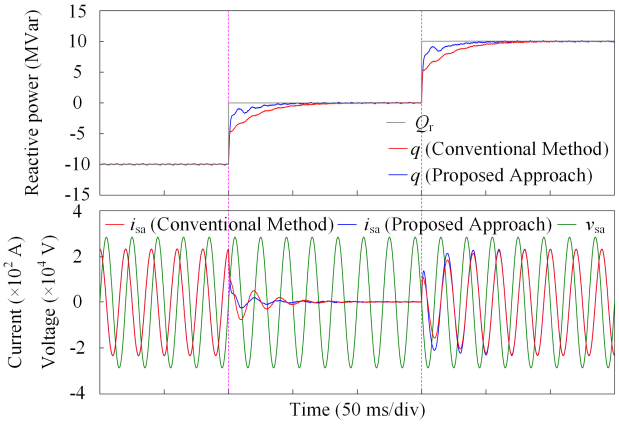

Fig. 18. Dynamic and steady-state performance of the STATCOM optimized by the conventional method and proposed approach.

that the trajectories do not enclose the (–1, 0j) point in both situations, which means the system becomes stable with the two sets of STATCOM controller parameters. The equivalent impedance ratio $Z_{eg}(s)Y_{ewf}(s)$ of the wind farm is further presented in Fig. 15 to obtain the quantitative stability margin. Compared to the impedance responses of $Z_{ewf}(s)$ (Case 2) in Fig. 7, the STATCOM optimized by the conventional method and proposed approach increases both the magnitude and phase responses of the equivalent impedance of the wind farm, which shift their intersections with $Z_{eg}(s)$ to higher frequencies (118.9 Hz and 102.4 Hz) with 17.74°- and 24.82°-phase margin, respectively. This indicates that the resonances in the wind farm will be mitigated when the STATCOM is optimized by the conventional method and proposed approach, and the STATCOM optimized by the proposed approach will provide more damping to the system and make it more robust.

Fig. 16 shows the simulation results of the injected currents and output powers of the wind farm for the STATCOM optimized by the conventional method and proposed approach. At the beginning of the simulation, the resonance occurs in the wind farm for the STATCOM without optimization, of which the controller parameters are shown in TABLE II. Then, the resonances are both effectively mitigated as the STATCOM controller parameters changed to those obtained by the conventional optimization method and proposed optimization approach in TABLE VI. Additionally, as observed in the dynamic process of the output powers, compared to the system for the STATCOM optimized by the conventional method, the amplitude of resonance in the system for the STATCOM optimized by the proposed approach is attenuated more greatly within a shorter settling time, which confirms the analysis in Fig. 15. The corresponding FFT results in Fig. 17 show each harmonic at 1 to 150 Hz of the injected currents of the wind farm does not exceed 0.01% of the fundamental in both situations when the system becomes fully stable.

The dynamic and steady-state performance of the STATCOM optimized by the conventional method and proposed approach are further examined by two steps in the reactive power reference Q_r from full-load for absorbing capacitive reactive power to no-load, and then from no-load to full-load for absorbing inductive reactive power, as presented in Fig. 18. It can be found that, compared to the situation of the STATCOM optimized by the conventional method, the reactive power q for the STATCOM optimized by the proposed approach tracks the step reference Q_r with faster dynamics and reaches the steady-state within two fundamental periods, and the corresponding transient current changes smoothly with smaller amplitude during the regulation process. Furthermore, the total harmonic distortion (THD) of the steady-state currents for the STATCOM optimized by the conventional method and proposed approach are 0.42% and 0.71%, respectively. It is noted that although the amplitude of harmonics in the phase current of the STATCOM optimized by the proposed approach is larger due to its lower magnitude responses of impedance in Fig. 13, it still meets the requirements of being less than 5%.

In summary, the STATCOM controller parameters optimized by the understanding-of-models-based method help to use the STATCOM to mitigate the system resonance, but

This article has been accepted for publication in a future issue of this journal, but has not been fully edited. Content may change prior to final publication. Citation information: DOI 10.1109/JESTPE.2020.3020434, IEEE Journal of Emerging and Selected Topics in Power Electronics

this optimization method is difficult to achieve an optimal design. On the contrary, the proposed optimization approach for the STATCOM impedance utilizes the PSO algorithm to solve the STATCOM controller parameters to obtain the maximum stability margin of the wind farm system under the constraints of the performance indices of each STATCOM control loop, which help the STATCOM achieve an optimal balance between its own performance and system stability. In addition, with the advantages of the simple structure and fast solution speed of the PSO algorithm, the proposed approach can be applied not only to the off-line optimization of the STATCOM impedance to avoid the risk of wind farm resonance during the planning phase, but also to the system-level real-time optimization of the STATCOM impedance with the help of online impedance identification techniques to enhance the wind farm damping in operation.

VI. Conclusion

The STATCOM is considered as an effective and cheap alternative to mitigate resonance in wind farms. To achieve so, based on the sequence impedance matrix models of the Type-IV WTG and STATCOM for the network modeling, a sequence impedance network-based stability analysis for practical wind farms was presented in this paper to accurately analyze the stability of wind farms and quantitatively evaluate the damping provided by the STATCOM. A case study for a typical wind farm in Western China with different operation conditions was presented and the simulation results have validated the effectiveness of the proposed stability analysis. More importantly, according to the analysis of the effects of the STATCOM control loop on its impedance, the STATCOM impedance characteristics at certain frequency ranges may be affected by multiple control loops, and such effects caused by each control loop are coupled with each other. Therefore, to enhance the stability of the wind farm using the STATCOM impedance, an intelligent parameter design-based impedance optimization approach of the STATCOM was proposed. The proposed approach uses the heuristic intelligence algorithm, where the PSO algorithm was exemplified, to solve for the STATCOM controller parameters to obtain the optimal stability margin. A comparison with the STATCOM controller parameters optimized by the conventional method was presented to demonstrate that the controller parameters obtained by the proposed approach not only help the STATCOM to achieve resonance mitigation, but also make the wind farm system more robust, while ensuring the basic dynamic and steady-state performance of the STATCOM.

Appendix A

$\mathbf{Y}_{\mathrm{lw}}$ is expressed as

$$\mathbf{Y}_{\mathrm{lw}}=\frac{1}{L_{\mathrm{w}}}\mathrm{diag}\left(\frac{1}{s-2\mathrm{j}\omega_{\mathrm{l}}},0,\frac{1}{s},\frac{1}{s+\mathrm{j}\omega_{\mathrm{l}}},0\right) \tag{A1}$$

$\mathbf{Z}_{\mathrm{dc}}$ is expressed as

$$\mathbf{Z}_{\mathrm{dc}}=\frac{3}{2C_{\mathrm{dc}}}\mathrm{diag}\left(0,\frac{1}{s-\mathrm{j}\omega_{\mathrm{l}}},0,0,\frac{1}{s+2\mathrm{j}\omega_{\mathrm{l}}}\right) \tag{A2}$$

$\mathbf{V}_{\mathrm{dc}}$ is a 5×5 diagonal matrix with the main diagonal element as V_{dc};

$\mathbf{M}_{\mathrm{w}}$ is a 5×5 tridiagonal matrix with the main diagonal elements as zero, the elements in the diagonal above the main diagonal as $M_{\mathrm{w1}}\mathrm{e}^{-\mathrm{j}\gamma_{\mathrm{w1}}}$, and the elements in the diagonal below the main diagonal as $M_{\mathrm{w1}}\mathrm{e}^{\mathrm{j}\gamma_{\mathrm{w1}}}$ (M_{w1} and γ_{w1} are the amplitude and phase of the Fourier coefficient of the modulation signal at f_1);

$\mathbf{I}_{\mathrm{w}}$ is a 5×5 tridiagonal matrix with the main diagonal elements as zero, the elements in the diagonal above the main diagonal as $I_{\mathrm{w1}}\mathrm{e}^{-\mathrm{j}\alpha_{\mathrm{w1}}}$, and the elements in the diagonal below the main diagonal as $I_{\mathrm{w1}}\mathrm{e}^{\mathrm{j}\alpha_{\mathrm{w1}}}$ (I_{w1} and α_{w1} are the amplitude and phase of the Fourier coefficient of the phase current at f_1);

$\mathbf{Q}_{\mathrm{w}}$ is expressed as

$$\begin{aligned}\mathbf{Q}_{\mathrm{w}}=\mathrm{diag}(&-H_{\mathrm{wi}}(s-\mathrm{j}\omega_{\mathrm{l}})-\mathrm{j}K_{\mathrm{wd}},0,-H_{\mathrm{wi}}(s-\mathrm{j}\omega_{\mathrm{l}})+\mathrm{j}K_{\mathrm{wd}},\\&-H_{\mathrm{wi}}(s+2\mathrm{j}\omega_{\mathrm{l}})-\mathrm{j}K_{\mathrm{wd}},0)\end{aligned} \tag{A3}$$

$\mathbf{P}_{\mathrm{w}}$ is a 5×5 zero matrix except for the (1, 3)-th and (3, 3)-th elements, denoted respectively as

$$\begin{aligned}&-\mathrm{e}^{-\mathrm{j}\varphi_{\mathrm{w1}}}G_{\mathrm{w}\theta}(s-\mathrm{j}\omega_{\mathrm{l}})\cdot\\&\{I_{\mathrm{w1}}\mathrm{e}^{-\mathrm{j}\alpha_{\mathrm{w1}}}[H_{\mathrm{wi}}(s-\mathrm{j}\omega_{\mathrm{l}})+\mathrm{j}K_{\mathrm{wd}}]+M_{\mathrm{w1}}\mathrm{e}^{-\mathrm{j}\gamma_{\mathrm{w1}}}\}\end{aligned} \tag{A4}$$

$$\begin{aligned}&\mathrm{e}^{-\mathrm{j}\varphi_{\mathrm{w1}}}G_{\mathrm{w}\theta}(s-\mathrm{j}\omega_{\mathrm{l}})\cdot\\&\{I_{\mathrm{w1}}\mathrm{e}^{\mathrm{j}\alpha_{\mathrm{w1}}}[H_{\mathrm{wi}}(s-\mathrm{j}\omega_{\mathrm{l}})-\mathrm{j}K_{\mathrm{wd}}]+M_{\mathrm{w1}}\mathrm{e}^{\mathrm{j}\gamma_{\mathrm{w1}}}\}\end{aligned} \tag{A5}$$

where $G_{\mathrm{w}\theta}(s)=T_{\mathrm{w}\theta}(s)/(1+V_{\mathrm{w1}}T_{\mathrm{w}\theta}(s))$ and $T_{\mathrm{w}\theta}(s)=H_{\mathrm{w}\theta}(s)/s$, V_{w1} and φ_{w1} are the amplitude and phase of the fundamental output terminal voltage;

$\mathbf{E}_{\mathrm{w}}$ is a 5×5 zero matrix except for the (1, 2)-th and (3, 2)-th elements, denoted respectively as

$$\frac{\mathrm{e}^{-\mathrm{j}\varphi_{\mathrm{w1}}}}{2}H_{\mathrm{wv}}(s-\mathrm{j}\omega_{\mathrm{l}})H_{\mathrm{wi}}(s-\mathrm{j}\omega_{\mathrm{l}}) \tag{A6}$$

$$\frac{\mathrm{e}^{\mathrm{j}\varphi_{\mathrm{w1}}}}{2}H_{\mathrm{wv}}(s-\mathrm{j}\omega_{\mathrm{l}})H_{\mathrm{wi}}(s-\mathrm{j}\omega_{\mathrm{l}}) \tag{A7}$$

Appendix B

$\mathbf{Y}_{\mathrm{l}}$ is expressed as

$$\mathbf{Y}_{\mathrm{l}}=\frac{1}{L}\mathrm{diag}\left(\frac{1}{s-2\mathrm{j}\omega_{\mathrm{l}}},0,\frac{1}{s},\frac{1}{s+\mathrm{j}\omega_{\mathrm{l}}},0\right) \tag{B1}$$

$\mathbf{Z}_{\mathrm{c}}$ is expressed as

$$\mathbf{Z}_{\mathrm{c}}=\frac{N}{C_{\mathrm{m}}}\mathrm{diag}\left(\frac{1}{s+\mathrm{j}n\omega_{\mathrm{l}}}\Big|_{n=-2,-1,0,1,2}\right) \tag{B2}$$

$\mathbf{V}_{\mathrm{i}}$ is a 5×5 matrix with the main diagonal element as V_{i0}, the $(n,n+2)|_{n=1,2,3}$-th element as $V_{\mathrm{i2}}\mathrm{e}^{-\mathrm{j}\beta_{\mathrm{i2}}}$, the $(n+2,n)|_{n=1,2,3}$-th element as $V_{\mathrm{i2}}\mathrm{e}^{\mathrm{j}\beta_{\mathrm{i2}}}$, and the rest element as zero (V_{i2} and β_{i2} are the amplitude and phase of the Fourier coefficient of the

module capacitor voltage at $2f_1$);

M is a 5×5 tri-diagonal matrix with the main diagonal elements as zero, the elements in the diagonal above the main diagonal as $M_1 e^{-j\gamma_1}$, and the elements in the diagonal below the main diagonal as $M_1 e^{j\gamma_1}$ (M_1 and γ_1 are the amplitude and phase of the Fourier coefficient of the insertion index at f_1);

I is a 5×5 tri-diagonal matrix with the main diagonal elements as zero, the elements in the diagonal above the main diagonal as $I_{s1} e^{-j\alpha_{s1}}$, and the elements in the diagonal below the main diagonal as $I_{s1} e^{j\alpha_{s1}}$ (I_{s1} and α_{s1} are the amplitude and phase of the Fourier coefficient of the phase current at f_1);

Q is a 5×5 matrix, of which all elements are zero except for $(1, n+1)|_{n=0,2}$ -th elements that is

$$\frac{(2-n)}{2}\left[H_i(s-j\omega_1)+jK_d\right]+ e^{-jn\varphi_{s1}}\left[\frac{K_i}{2}+(1-n)\frac{3V_{s1}}{4}G_Q(s-j\omega_1)\right] \tag{B3}$$

the $(3, n+1)|_{n=0,2}$ -th elements that is

$$\frac{n}{2}\left[H_i(s-j\omega_1)-jK_d\right]+ e^{j(2-n)\varphi_1}\left[\frac{K_i}{2}+(n-1)\frac{3V_{s1}}{4}G_Q(s-j\omega_1)\right] \tag{B4}$$

and the (4, 4)-th element that is

$$H_i(s+2j\omega_1)+jK_d+\frac{K_i}{2}+\frac{3V_{s1}}{4}G_Q(s+2j\omega_1) \tag{B5}$$

where $G_Q(s) = H_Q(s)H_i(s)$ and φ_{s1} is the phase of the fundamental output terminal voltage;

P is a 5×5 zero matrix except for the (1, 3)-th and (3, 3)-th elements, denoted respectively as

$$e^{-j\varphi_{s1}}\{G_\theta(s-j\omega_1)[I_{s1}e^{-j\alpha_{s1}}(H_i(s-j\omega_1)+jK_d)-M_1e^{-j\gamma_1}+ \frac{I_{s1}(e^{-j\alpha_{s1}}-e^{j(\alpha_{s1}-2\varphi_{s1})})}{2}K_i]+\frac{3I_{s1}(e^{-j\alpha_{s1}}-e^{j(\alpha_{s1}-2\varphi_{s1})})}{4}G_Q(s-j\omega_1)\} \tag{B6}$$

$$-e^{-j\varphi_{s1}}\{G_\theta(s-j\omega_1)[I_{s1}e^{j\alpha_{s1}}(H_i(s-j\omega_1)-jK_d)-M_1e^{j\gamma_1}+ \frac{I_{s1}(e^{j\alpha_{s1}}-e^{-j(\alpha_{s1}-2\varphi_{s1})})}{2}K_i]-\frac{3I_{s1}(e^{j\alpha_{s1}}-e^{-j(\alpha_{s1}-2\varphi_{s1})})}{4}G_Q(s-j\omega_1)\} \tag{B7}$$

where $G_\theta(s) = T_\theta(s) / (1+V_{s1}T_\theta(s))$ and $T_\theta(s) = H_\theta(s) / s$;

E is a 5×5 zero matrix except for the $(n+1, n+2)|_{n=0,2}$ -th elements, denoted as

$$\frac{e^{-j\varphi_{s1}}}{2N}[K_iH_{pv}(s+j(n-1)\omega_1)+ \frac{(2-n)}{2}H_v(s-j\omega_1)H_i(s-j\omega_1)] \tag{B8}$$

and $(n+3, n+2)|_{n=0,2}$ -th elements, denoted as

$$\frac{e^{j\varphi_{s1}}}{2N}[K_iH_{pv}(s+j(n-1)\omega_1)+ \frac{(2-n)}{2}H_v(s-j\omega_1)H_i(s-j\omega_1)] \tag{B9}$$

REFERENCES

[1] S. W. Mohod and M. V. Aware, "A STATCOM-control scheme for grid connected wind energy system for power quality improvement," *IEEE Syst. J.*, vol. 4, no. 3, pp. 346-352, Sept. 2010.

[2] L. Wang and D. Truong, "Stability enhancement of DFIG-based offshore wind farm fed to a multi-machine system using a STATCOM," *IEEE Trans. Power Syst.*, vol. 28, no. 3, pp. 2882-2889, Aug. 2013.

[3] W. Qiao, G. K. Venayagamoorthy and R. G. Harley, "Real-time implementation of a STATCOM on a wind farm equipped with doubly fed induction generators," *IEEE Trans. Ind. Appl.*, vol. 45, no. 1, pp. 98-107, Jan.-Feb. 2009.

[4] A. Moharana, R. K. Varma and R. Seethapathy, "SSR alleviation by STATCOM in induction-generator-based wind farm connected to series compensated line," *IEEE Trans. Sustainable Energy*, vol. 5, no. 3, pp. 947-957, Jul. 2014.

[5] D. Shu, X. Xie, H. Rao, X. Gao, Q. Jiang and Y. Huang, "Sub- and super-synchronous interactions between STATCOMs and weak ac/dc transmissions with series compensations," *IEEE Trans. Power Electron.*, vol. 33, no. 9, pp. 7424-7437, Sept. 2018.

[6] H. Liu, X. Xie, J. He, T. Xu, Z. Yu, C. Wang, and C. Zhang, ''Subsynchronous interaction between direct-drive PMSG based wind farms and weak AC networks,'' *IEEE Trans. Power Syst.*, vol. 32, no. 6, pp. 4708–4720, Nov. 2017.

[7] J. Sun, M. Li, Z. Zhang, T. Xu, J. He, H. Wang, and G. Li, "Renewable energy transmission by HVDC across the continent: system challenges and opportunities," *CSEE J. Power Energy Syst.*, vol. 3, no. 4, pp. 353-364, Dec. 2017.

[8] B. Wen, D. Dong, D. Boroyevich, R. Burgos, P. Mattavelli, and Z. Shen, "Impedance-based analysis of grid-synchronization stability for three-phase paralleled converters," *IEEE Trans. Power Electron*., vol. 31, no. 1, pp. 26-38, Jan. 2016.

[9] S. Shah and L. Parsa, "Impedance modeling of three-phase voltage source converters in dq, sequence, and phasor domains," *IEEE Trans. Energy Convers.*, vol. 32, no. 3, pp. 1139-1150, Sept. 2017.

[10] X. Wang, L. Harnefors, and F. Blaabjerg, "Unified impedance model of grid-connected voltage-source converters," *IEEE Trans. Power Electron.*, vol. 33, no. 2, pp. 1775-1787, Feb. 2018.

[11] I. Vieto and J. Sun, "Sequence impedance modeling and analysis of type-III wind turbines," *IEEE Trans. Energy Convers.*, vol. 33, no. 2, pp. 537-545, Jun. 2018.

[12] S. Shah, P. Koralewicz, V. Gevorgian, R. Wallen, K. Jha, D. Mashtareet, R. Burra, and L. Parsa, "Large-signal impedance-based modeling and mitigation of resonance of converter-grid systems," *IEEE Trans. Sustainable Energy*, vol. 10, no. 3, pp. 1439-1449, July 2019.

[13] X. Chen, Y. Zhang, S. Wang, J. Chen and C. Gong, "Impedance-phased dynamic control method for grid-connected inverters in a weak grid," *IEEE Trans. Power Electron.*, vol. 32, no. 1, pp. 274-283, Jan. 2017.

[14] I. Vieto, G. Li and J. Sun, "Behavior, modeling and damping of a new type of resonance involving type-III wind turbines," in *Proc. IEEE 19th Workshop Control Model. Power Electron.*, Jun. 2018, pp. 1-8.

[15] H. Liu and X. Xie, "Impedance network modeling and quantitative stability analysis of sub-/super-synchronous oscillations for large-scale wind power systems," *IEEE Access*, vol. 6, pp. 34431-34438, Jun. 2018.

[16] J. Lyu, X. Cai, and M. Molinas, "Frequency domain stability analysis of MMC-based HVDC for wind farm integration." *IEEE J. Emerg. Sel. Topics Power Electron.*, vol.4, no. 1, pp. 141-151, Mar. 2016.

[17] Y. Zhang, X. Chen and J. Sun, "Impedance modeling and control of STATCOM for damping renewable energy system resonance," in *Proc. IEEE Energy Convers. Congr. and Expo.*, Oct. 2017, pp. 3295-3302.

[18] E. Ebrahimzadeh, F. Blaabjerg, X. Wang and C. L. Bak, "Harmonic stability and resonance analysis in large PMSG-based wind power plants," *IEEE Trans. Sustainable Energy*, vol. 9, no. 1, pp. 12-23, Jan. 2018.

[19] M. Lu, Y. Yang, B. Johnson and F. Blaabjerg, "An interaction-admittance model for multi-inverter grid-connected systems," *IEEE Trans. Power Electron.*, vol. 34, no. 8, pp. 7542-7557, Aug. 2019.
[20] H. Liu, X. Xie and W. Liu, "An oscillatory stability criterion based on the unified-frame impedance network model for power systems with high-penetration renewables," *IEEE Trans. Power Syst.*, vol. 33, no. 3, pp. 3472-3485, May 2018.
[21] H. Wang, I. Vieto and J. Sun, "A method to aggregate turbine and network impedances for wind farm system resonance analysis," in *Proc. IEEE 19th Workshop Control Model. Power Electron.*, Jun. 2018, pp. 1–8.
[22] I. Vieto and J. Sun, "Sequence impedance modeling and converter-grid resonance analysis considering dc bus dynamics and mirrored harmonics," in *Proc. IEEE 19th Workshop Control Model. Power Electron.*, Jun. 2018, pp. 1–8.
[23] M. Kazem Bakhshizadeh, X. Wang, F. Blaabjerg, J. Hjerrild, Ł. Kocewiak, C. Leth Bak, and B. Hesselbæk, "Couplings in phase domain impedance modeling of grid-connected converters," *IEEE Trans. Power Electron.*, vol. 31, no. 10, pp. 6792-6796, Oct. 2016.
[24] Y. Zhang, X. Chen and J. Sun, "Sequence impedance modeling and analysis of MMC in single-star configuration," *IEEE Trans. Power Electron.*, vol. 35, no. 1, pp. 334-346, Jan. 2020.
[25] C. Li, R. Burgos, B. Wen, Y. Tang and D. Boroyevich, "Stability analysis of power systems with multiple STATCOMs in close proximity," *IEEE Trans. Power Electron.*, vol. 35, no. 3, pp. 2268-2283, March 2020.
[26] N. Voraphonpiput and S. Chatratana, "STATCOM analysis and controller design for power system voltage regulation," in *Proc. IEEE/PES Transmission and Distribution Conference and Exposition: Asia and Pacific*, Aug. 2005, pp. 1-6.
[27] B. Chen and Y. Hsu, "An analytical approach to harmonic analysis and controller design of a STATCOM," *IEEE Trans. Power Del.*, vol. 22, no. 1, pp. 423-432, Jan. 2007.
[28] H. Akagi, S. Inoue and T. Yoshii, "Control and performance of a transformerless cascade PWM STATCOM with star configuration," *IEEE Trans. Ind. Appl.*, vol. 43, no. 4, pp. 1041-1049, July-aug. 2007.
[29] C. Li, R. Burgos, B. Wen, Y. Tang and D. Boroyevich, "Analysis of STATCOM small-signal impedance in the synchronous d-q frame," *IEEE J. Emerg. Sel. Topics Power Electron.*, vol. 8, no. 2, pp. 1894-1910, June 2020.
[30] A. Rygg, M. Molinas, C. Zhang, and X. Cai, "A modified sequence-domain impedance definition and its equivalence to the dq-domain impedance definition for the stability analysis of AC power electronic systems," *IEEE J. Emerg. Sel. Topics Power Electron.*, vol. 4, no. 4, pp. 1383-1396, Dec. 2016.
[31] Abdelhay A. Sallam and Om P. Malik, "Power system stability: modelling, analysis and control", *the Institution of Engineering and Technology*, 2015.
[32] C. Zhang, X. Cai, A. Rygg, and M. Molinas, "Sequence domain SISO equivalent models of a grid-tied voltage source converter system for small-signal stability analysis," *IEEE Trans. Energy Convers.*, vol. 33, no. 2, pp. 741-749, June 2018.
[33] J. Kennedy and R. Eberhart, "Particle swarm optimization," in *Proc. International Conference on Neural Networks*, 1995, pp. 1942-1948.
[34] Y. Tang, P. Ju, H. He, C. Qin, and F. Wu, "Optimized control of DFIG-based wind generation using sensitivity analysis and particle swarm optimization," *IEEE Trans. Smart Grid*, vol. 4, no. 1, pp. 509-520, March 2013.
[35] M. Chouket, A. Abdelkafi, and L. Krichen, "Wind turbine PI controller's optimization using PSO algorithm," in *Proc. 15th International Multi-Conference on Systems, Signals & Devices*, 2018, pp. 1287-1292.
[36] N. Nayak, S. Mishra, S. Choudhury, and P. K. Rout, "Optimal design of VSC based HVDC using particle swarm optimization technique," in *Proc. 2nd International Conference on Power, Control and Embedded Systems*, 2012, pp. 1-5.
[37] P. Mc Namara, R. R. Negenborn, B. De Schutter, and G. Lightbody, "Optimal coordination of a multiple HVDC link system using centralized and distributed control," *IEEE Trans. Control Syst. Technol.*, vol. 21, no. 2, pp. 302-314, Mar. 2013.

Yang Zhang (S'17) was born in Fujian Province, China, in 1989. He received the B.S. and M.S. degrees in electrical engineering and automation from Nanjing University of Aeronautics and Astronautics, Nanjing, China, where he is currently working toward the Ph.D. degree in electrical engineering.

His main research interests include the renewable generation system modeling, stability analysis and control.

Yongheng Yang (SM'17) received the B.Eng. degree in electrical engineering and automation from Northwestern Polytechnical University, Shanxi, China, in 2009 and the Ph.D. degree in electrical engineering from Aalborg University, Aalborg, Denmark, in 2014.

He was a postgraduate student with Southeast University, China, from 2009 to 2011. In 2013, he spent three months as a Visiting Scholar at Texas A&M University, USA. Currently, he is an Associate Professor with the Department of Energy Technology, Aalborg University, where he also serves as the Vice Program Leader for the research program on photovoltaic systems. His current research is on the integration of grid-friendly photovoltaic systems with an emphasis on the power electronics converter design, control, and reliability.

Dr. Yang is the Chair of the IEEE Denmark Section. He serves as an Associate Editor for several prestigious journals, including the IEEE TRANSACTIONS ON INDUSTRIAL ELECTRONICS, the IEEE TRANSACTIONS ON POWER ELECTRONICS, and the IEEE Industry Applications Society (IAS) Publications. He is a Subject Editor of the *IET Renewable Power Generation* for Solar Photovoltaic Systems. He was the recipient of the 2018 *IET Renewable Power Generation* Premium Award and was an Outstanding Reviewer for the IEEE TRANSACTIONS ON POWER ELECTRONICS in 2018.

Xin Chen (S'99-M'04) received the B.S. and Ph.D. degrees in electrical engineering from Nanjing University of Aeronautics and Astronautics, Nanjing, China, in 1996 and 2001, respectively.

He is a Professor of Department of Electrical Engineering, Nanjing University of Aeronautics and Astronautics. He was a Chief Engineer (2001-2003) in Power Division of ZTE Corporation, and he was a Visiting Scholar (2010-2011) at the Rensselaer Polytechnic Institute, Troy, USA. His current research interests include modeling, control and stability of distributed generation and microgrid systems.

Chunying Gong (M'07) was born in Zhejiang, China, in 1965. She received the B.S., M.S., and Ph.D. degrees in electrical engineering from Nanjing University of Aeronautics and Astronautics (NUAA), Nanjing, China, in 1984, 1990, and 1993, respectively.

From 1984 to 1987, she was an Electrical Assistant Engineer with Chengdu Aircraft Design and Research Institute. In 1993, she joined the College of Automation Engineering, NUAA, as a Lecturer, where, in 1996 and 2004, she became an Associate Professor and a Professor, respectively. In 2009, she was a Visiting Scholar in the Department of Electrical, Computer, and Systems Engineering, Rensselaer Polytechnic Institute, New York, USA. She is the author or coauthor of more than 100 technical papers published in journals and conference proceedings. Her research focuses on static inverters, power electronic systems stability and power quality, renewable energy, and distributed generation.